Biochemical and structural analysis of N-myristoyltransferase mediated protein tagging

Paul Monassa, Frédéric Rivière, Cyril Dian, Frédéric Frottin, Carmela Giglione, Thierry Meinnel

CHAPTER FIVE

Biochemical and structural analysis of N-myristoyltransferase-mediated protein tagging

Paul Monassa[iD,a,£], Frédéric Rivière[iD,a,1,£], Cyril Dian[iD,a], Frédéric Frottin[iD,a], Carmela Giglione[iD,@,a], Thierry Meinnel[iD,@,a,*]

[a] Université Paris Saclay, CEA, CNRS, Institute for Integrative Biology of the Cell (I2BC), 91198 Gif-sur-Yvette cedex, France

Running title: N-myristoylation-related biochemical methods

Correspondence: carmela.giglione@i2bc.paris-saclay.fr (C. Giglione) or thierry.meinnel@i2bc.paris-saclay.fr (T. Meinnel)

[iD] ORCID iD 0001-6366-1904 (F. Rivière); 0003-4713-8069 (P. Monassa); 0002-6349-3901 (C. Dian); 0002-2756-7838 (F. Frottin); 0002-7475-1558 (C. Giglione); 0001-5642-8637 (T. Meinnel)

[@]twitter @giglionelab (C. Giglione); @meinnel (T. Meinnel)

[£] These authors contributed equally

Present address

[1] Karolinska Institutet, Department of Biosciences and Nutrition, 14183 Huddinge, Sweden

Keywords: Protein acylation; lysine; myristoylation; acetylation; *N*-myristoyltransferase; N-terminus; glycine; protein modification; fatty acid

Contents

Abstract

N-terminal myristoylation is an essential eukaryotic modification crucial for cellular homeostasis in the context of many physiological processes. Myristoylation is a lipid modification resulting in a C14 saturated fatty acid addition. This modification is challenging to capture due to its hydrophilicity, low abundance of target substrates, and the recent discovery of unexpected NMT reactivity including myristoylation of lysine side chains and N-acetylation in addition to classical N-terminal Gly-myristoylation. This chapter details the high-end approaches developed to characterize the different features of N-myristoylation and its targets through *in vitro* and *in vivo* labeling.

1. Introduction

N-myristoyltransferases (glycylpeptide N-tetradecanoyltransferases, myristoyl CoA:protein N-myristoyltransferases, NMT; EC 2.3.1.97) are a class of essential enzyme catalysts of protein myristoylation. NMTs target N-terminal glycines (Gly-myristoylation) usually unmasked by co-translational methionine excision (Giglione & Meinnel, 2022; Meinnel, Dian, & Giglione, 2020). A general scheme of classical NMT reactivity is provided in **Fig. 1A**. The initiator methionine is removed by methionine aminopeptidases (MetAPs, EC:3.4.11.18). Most eukaryotes express two MetAPs, MetAP1 and MetAP2, both of which display high cleavage efficiency of Met-Gly peptide bonds (Frottin et al., 2006; Giglione, Boularot, & Meinnel, 2004). Post-translational proteolytic cleavages induced by caspases (EC:3.4.22.xx) in the context of apoptosis in metazoans may also expose new N-terminal glycines previously embedded within the polypeptide sequence that may similarly undergo Gly-myristoylation (Martin, Beauchamp, & Berthiaume, 2011; Thinon et al., 2014). As caspase 3 (EC:3.4.22.56) restricts new N-termini to only small residues (i.e., Ala, Gly, Asn, and Ser),

its cleavage specificity is well suited for this purpose and is the major post-translational provider of post-translational Gly-myristoylation (Meinnel, 2022; Rivière et al., 2022). Two percent of multicellular eukaryote proteins are predicted to undergo Gly-myristoylation, mostly of co-translational origin (Castrec et al., 2018; Meinnel, 2022; Meinnel et al., 2020).

However, experimental proof of myristoylation only exists for a minority – most from human – of protein targets. Evidence of myristoylation of a novel target protein is often indirect, for instance by establishing protein localization with or without the N-terminal Gly, which is usually substituted with an Ala (Traverso et al., 2013b). This so-called G2A substitution is known to inhibit myristoylation (Gordon, Duronio, Rudnick, Adams, & Gokel, 1991). Robust biochemical approaches for investigating NMT targeting were initially reported in the 1990s (see, for instance, (Rudnick, Duronio, & Gordon, 1992) and this series, volume 250, chapters 29-37, (Casey & Buss, 1995)). However, in the early 2010s, new technologies emerged to study myristoylation including state-of-the-art mass spectrometry, click and bioorthogonal chemistry, and new structural approaches. This chapter is dedicated to the main approaches available for deciphering the modification state of NMT targets.

2. Materials, reagents, and buffers

2.1 Equipment

2.1.1 Instruments

● Matrix-assisted laser desorption/ionization-time of flight (MALDI-TOF) mass spectrometer for mass spectrometry (MS) and MS/MS spectra acquisition (AB Sciex LLC; MALDI-TOF/TOF 5800 instrument).

126 ● Nano liquid chromatography-coupled electrospray mass spectrometer (Dionex UltiMate
127 3000; AB Sciex LLC, TripleTOF 4600) for exact mass determination of entire proteins larger
128 than 30 kDa.
129 ● Multicolor fluorescence imager (Typhoon RGB Biomolecular Imager, GE Healthcare)
130 equipped with 532 nm-excited fluorescence and 580 nm bandpass (580 BP 30) filter for
131 wavelength emission range of 565–595 nm suited to Cy3 or TAMRA fluorochromes. The 633
132 nm-excited fluorescence with 670 nm bandpass (670 BP 30) for wavelength emission detection
133 range of 655–685 nm is suited to Cy5-type probe detection. Note that Typhoon Trio imagers
134 offer additional chemiluminescence detection.
135 ● Chemiluminescence and staining imaging system equipped with Chemi/UV/Stain-Free tray
136 (ChemDoc Touch, Bio-Rad).
137 ● Ultrasonic sonicator (Q700, Qsonica) equipped with a 12 mm Macrotip (amplitude 120 µm).

138 *2.1.2 Small items*

139 ● Precast gels (12%) for electrophoretic separation in standard Tris-glycine buffer (Mini-
140 PROTEAN TGX, Bio-Rad, 4561043).
141 ● Polyvinylidene fluoride (PVDF) immunoblot membranes (Immun-Blot Low Fluorescence
142 membranes, Bio-Rad, 1620260-4).
143 ● Bradford assay kit (Bio-Rad, 500001) for protein quantification determined against a
144 standard bovine serum albumin (BSA) calibration curve (Bradford, 1976).
145 ● Lipofectamine 3000 (Thermo Fisher Scientific, L3000015) for cell transfection.
146 ● Polyethylene glycol 6000 (Sigma-Aldrich, 81260) for protein crystallization.

147 **2.2 Plasmids, strains, and growth medium for protein expression**

148 *2.2.1 Plasmids*

● pET28b tobacco etch virus (TEV) vector (LifeScience Market, PVT10578) featuring a 6-His tag. We use a similar but in-lab-engineered version of pET28a TEV featuring a 10-His tag as described below. Expression requires kanamycin (50 µg/mL) in the growth medium.

● pET16b (Novagen, 69662). Expression requires 50 µg/mL ampicillin in the growth medium.

● pETM30 is a pET28b derivative featuring an N-terminal-GST fusion (Dümmler, Lawrence, & De Marco, 2005). Expression requires kanamycin (50 µg/mL) in the growth medium.

● pET21-ARF6-His6, a kind gift from M. Franco (IPMC, Nice, France) for ARF6-His overexpression and purification in *E. coli*. ARF6-His6 is 21.0 kDa (ARF6 is 19.9 kDa).

● pJAF211 (Addgene, 52407) for ARF6-Flag overexpression in mammalian cells. The cDNA sequence originates from mice and encodes the same peptide chain as in humans. The Flag-tag is at the C-terminal. ARF6-Flag is 23.8 kDa.

● pETDuet-1 (Novagen) for dual overexpression of both NMT and target protein of interest cDNAs.

2.2.2 Bacterial growth

● Rosetta 2-DE3pLys bacterial strain (Novagen). Genotype is F^- *ompT gal dcm lon hsdS*$_B$(r_B^- m_B^-) λ(DE3 [*lacI lacUV5-T7p07 ind1 sam7 nin5*]) [*malB*$^+$]$_{K\text{-}12}$(λ^S)). pLysSRARE produces T7 lysozyme and tRNA genes to supplement *E. coli* rare codons AGG, AGA, AUA, CUA, CCC, and GGA. Add chloramphenicol (34 µg/mL) to ensure plasmid propagation in the growth medium.

● 2xTY growth medium. Mix 16 g Bacto Tryptone, 10 g Bacto Yeast Extract, and 5 g NaCl in 900 mL distilled H_2O. Adjust the pH to 7.0 with NaOH and finally adjust to 1 L with distilled H_2O. Sterilize by autoclaving.

2.3 Enzymes

2.3.1 Commercial

● Acyl-CoA synthetase (ACS; EC 6.2.1.3) from *Pseudomonas sp.* (Creative Enzymes, NATE-1712; 15 U/mg; 1000 U). Dilute the sample to 1 U/µL in 5 mM Tris-HCl pH 7.4, 1 mM DTT, 55% glycerol for storage at -20°C. ACS catalyzes the reaction shown in **Fig. 1B**.

● Recombinant TEV (rTEV, EC 3.4. 22.44) protease (Genscript, Z03030, 10 U/µl); rTEV contains the 231 amino acid sequence of TEV fused to an N-terminal His tag. It cleaves the Glu-Asn-Leu-Tyr-Phe-Gln/[Gly/Ser] sequence (Kapust et al., 2001) and can be removed by nickel cation affinity assays. To reduce purchase costs, TEV and rTEV can also be overexpressed and easily purified from recombinant plasmid vectors (Enríquez-Flores et al., 2022; Nautiyal & Kuroda, 2018).

2.3.2 NMTs

In this section, we describe the NMT preparations required for kinetic or structural analysis. Protein concentrations are measured with the aforementioned Bio-Rad kit. Purity needs to be >95% for kinetic analysis and >99.9% for crystallization purposes. We usually clone into a pET16b featuring a Factor Xa protease cleavage or a pET28b derivative vector featuring an N-terminal 10x His tag fused with a TEV protease cleavage site. Expression is performed at 22°C in Rosetta2-DE3pLysS bacterial cells. The protocol reported below relates to HsNMT1[*l*] (Dian et al., 2020) but may be used for any NMT (see below).

● Like Factor Xa, the TEV protease-cleavable linker of the inter-domain (CATCACCATCACCATCACCATCACCATCACGAGAATCTTTATTTTCAGGGC; encoding here Glu-Asn-Leu-Tyr-Phe-Gln/Gly fused in-frame downstream of the His-tag and upstream of the start of the sequence of interest) permits *in vitro* cleavage of the His-tag from the expressed NMT if the pET28-derived vector is used for protein purification. Upon cleavage, the His-tag is removed from the NMT sample of interest by taking advantage of a second affinity column on the same resin. The NMT is easily recovered, as it is not retained

and elutes with the flow-through. Unlike TEV or Factor Xa, the rTEV protease is equipped with a His-tag and can also be retained on the second affinity column, allowing its removal and fine purification of an NMT version devoid of protease contaminants, especially useful for crystallization purposes.

● NMTs are easy to overexpress in *Escherichia coli* and purify in two steps, taking advantage of the N-terminal tags. C-terminal tags need to be avoided, as the C-terminal carboxylate of NMTs acts as the catalytic base and cannot be engaged in another peptide bond (Dian et al., 2020). N-terminal deletions of NMT sequences up to the B'A' domain can be achieved without modification of the catalytic parameters. Trimming of this domain modifies the catalytic mechanism and tends to increase the turnover number (Dian et al., 2020).

● After growth at 37°C in 2 L 2x TY medium supplemented with the *ad hoc* antibiotics until 0.4-0.5 OD_{600}, the temperature is reduced to 22°C for 30 min to reach 0.7-0.9 OD_{600}. Bacteria are induced with 0.4 mM isopropyl-1-thio-β-D-galactopyranoside (IPTG) and grown for another 20 h at 22°C under vigorous shaking. Cells are harvested by centrifugation and lysed by sonication (amplitude 50%, 10 s on and 30 s off) for 90 s at 4°C after resuspension in 10 mL/per g of cell paste in 20 mM Tris–HCl (pH 8.0), 0.5 M NaCl, 5 mM 2-mercaptoethanol, and 5 mM imidazole (buffer C) supplemented with 1 mg/mL lysozyme and 5 µL benzonase. After centrifugation at 40,000 x g, the clarified lysate is loaded at 3 mL/min onto an immobilized nickel ion affinity chromatography column (HisTrap Crude FF, 5 mL, GE Healthcare) and washed with buffer C with 25 mM imidazole. Elution is carried out at 2 mL/min with buffer C plus 0.25 M imidazole with a linear gradient.

The pool of purified protein is next dialyzed overnight against 20 mM Tris-HCl (pH 8.9), 150 mM NaCl, 25 mM imidazole, and 5 mM 2-mercaptoethanol in the presence of TEV protease (1 mg per 15 mg purified protein). His-tag-free HsNMT1 is purified with a HisTrap Crude FF column. The flow-through with HsNMT1 is diluted five times in 20 mM Tris-HCl

(pH 8.9) and 1 mM DTT (buffer B) and applied to an anion exchange chromatography column (HiTrap Q FF, 5 mL, GE Healthcare). HsNMT1 is eluted with buffer B supplemented with 0.2 M NaCl. Finer purification of some NMTs might require a final gel filtration step, but we have not needed this for our crystallization of HsNMT1.

● Highly purified NMT fractions are pooled, concentrated to 15–30 mg/ mL with an Amicon centrifugal filtration device (Merck Millipore) in 20 mM Tris–HCl (pH 8.0), 0.2 M NaCl, 1 mM DTT, and stored at -80°C before crystallization trials. Protein samples for kinetic analysis are stored at -20°C in the same buffer plus 55% glycerol.

● Human NMT (HsNMT1). The HsNMT1(*l*) isoform containing residues 81-496 corresponds to the major isoform (Pierre et al., 2007). We cloned HsNMT1(*l*) into pET16b as an N-terminal His-tag fusion (Pierre et al., 2007), and the recombinant protein was expressed and purified as described (Castrec et al., 2018). Isoform HsNMT1(*s*) containing residues 99-496 was cloned into pET28b and purified as described (Dian et al., 2020).

● Full-length HsNMT2, AtNMT, PfNMT, and ScNMT can be expressed and purified according to similar protocols as previously described (Castrec et al., 2018; Traverso, Giglione, & Meinnel, 2013a).

2.3.3 IpaJ protease

IpaJ (EC:3.4.22) is a cysteine protease displaying tight cleavage specificity for myristoyl-glycine-starting peptides that hydrolyzes the peptide bond immediately following the glycine residue (Burnaevskiy et al., 2013; Burnaevskiy, Peng, Reddick, Hang, & Alto, 2015; Rivière et al., 2022). A scheme of the reaction catalyzed by IpaJ is provided in **Fig. 1C**.

A truncated (i.e., devoid of the N-terminal secretion peptide) and more soluble (3M) variant of the open reading frame of *Shigella flexneri* protease IpaJ is cloned into pETM30 as a fusion with a N-terminal His-tag and glutathione S-transferase (GST) as described (Rivière

et al., 2022). IpaJ is produced from Rosetta2-DE3pLysS cells. Bacteria are grown in 1 L of 2x TY medium supplemented with kanamycin (50 µg/mL) and chloramphenicol (34 µg/mL) at 37°C under vigorous shaking. Protein overexpression is induced with 0.5 mM IPTG at OD_{600}=0.8. Cells are transferred at 20°C and grown for 20 h. Cells are centrifuged at 5,000 x *g* and the pellet resuspended (10 mL/g) in lysis buffer (20 mM Tris pH 8.0, 0.2 M NaCl, 5 mM 2-mercaptoethanol, 5 mM imidazole, 5% glycerol). Cells are lysed with a sonicator (amplitude 50%, 10 s on and 30 s off) for 3 min at 4°C. The sample is then centrifuged at 40,000 x *g* (Rotor JA25-50, Beckman Coulter) for 20 min and the pellet discarded. The supernatant is loaded on a Ni-IMAC-HisTrap™ FF 5 mL column (GE Healthcare) at 3 mL/min; elution is achieved with a liner 0-0.5 M imidazole gradient run over 100 ml. Purified proteins are dialyzed using Spectra-Por7 semi-permeable dialysis membranes (8 kDa cut-off; Thermo Fisher Scientific) for 48 h against conservation buffer (20 mM Tris pH 8.0, 0.2 M NaCl, 5 mM DTT, 55% glycerol) at 4°C. The sample is stored at -20°C.

2.4 Reagents

2.4.1 Fatty acyl derivatives

● Myristoyl-CoA lithium salt (Sigma-Aldrich, M4414) MM = 977.9 g/mol; 5 mg diluted in 25.565 mL. Stock solutions (0.2 mM) are prepared in 10 mM sodium acetate, pH 5.6, and 1% Triton X-100, except for MALDI analysis, where cholate is used instead of Triton to reduce background (see below). The low pH prevents slow CoA hydrolysis.

● 80% pure myristoyl-CoA lithium salt (Sigma-Aldrich, M4414) MM = 977.9 g/mol; 5 mg diluted in 0.511 mL in 50% DMSO (final concentration 10 mM), e.g., for use in crystallization trials.

● Acetyl-CoA, >93% pure (Sigma-Aldrich, A2056).

● Myristic acid (Sigma-Aldrich, M3128).

● Alkynyl myristic acid (Myr-Alk; Click Chemistry Tools, 1164-100).

● Azido myristic acid (Myr-Az; Click Chemistry Tools, 1345-100).

● Radioactive myristoyl-CoA (^{3}H or ^{14}C), which must be ordered as a custom synthesis, e.g., from Selcia, Moravek Biochemicals Inc., Quotient Sciences, or ViTrax or prepared as described in §3.1 from radiolabeled myristic acid (Moravek Inc, MC118 or MT918).

2.4.2 Peptides

Custom peptides octapeptides of any sequence are all from GenScript Biotech (Rijswijk, Netherlands).

2.4.3 Reactants for gel imaging

● Pre-stained protein ladder 10-250 kDa (PageRuler Plus, Thermo Fisher, 26620).

● TAMRA-PEG3-azide (BroadPharm, BP-22479) for in-gel imaging alkyne-tagged proteins by click chemistry. The TAMRA excitation peak corresponds to the Cy3 laser line and is fully compatible with parallel Cy5 detection.

● TAMRA DBCO (Click Chemistry Tools, A131-5) is a reactive probe used for imaging alkyne-tagged biomolecules via a copper-free click reaction.

● Biotin-PEG3-Azide (Thermo Fisher Scientific, J64996.MB; Sigma-Aldrich, 762024).

● TAMRA-biotin-PEG3-azide (Click Chemistry Tools, 1048).

● AlexaFluor Streptavidin 635 (Thermo Fisher Scientific, S32364) for fluorescence detection of proteins clicked with a biotin-PEG3-azide probe after blotting on PVDF membranes.

● ARF6-specific rabbit polyclonal antibody (Bethyl Laboratories, Inc; A305-238A).

● Beads coupled to Flag-tag antibody from the µMACS™ DYKDDDDK Isolation Kit (Miltenyi Biotec).

● NMT inhibitor IMP-1088 (Cayman Chemical Company, 25366) or DDD85646 (Cayman Chemical Company, 13839).

2.5 Buffer components

2.5.1 For storage at room temperature

● $MgCl_2$ stock 100 mM q.s. 50 mL; MM = 292.24 g/mol; 1.0165 g in 50 mL.

● Triton X-100 10% q.s. 15 mL; dilute use 1.5 mL Triton X-100 solution (Sigma-Aldrich, 93443).

● Ethylenediaminetetraacetic acid 0.5 M (EDTA) q.s. 100 mL; MM = 203.3 g/mol (Sigma-Aldrich, 03609). Add 101.6 g in H_2O and dissolve, taking advantage of NaOH addition (high concentration or chips) to reach pH 8 and allow complete solubilization in 100 mL final volume.

● 4x Laemmli buffer is 4% SDS, 20% glycerol, 10% 2-mercaptoethanol, 0.004% bromophenol blue, and 0.125 M Tris HCl, pH 6.8.

● Phosphate Buffer Saline (PBS) buffer is 137 mM NaCl, 27 mM KCl, 10 mM Na_2PO_4, 18 mM, K_2PO_4 and is adjusted to pH 7.4.

2.5.2 For storage at -20°C

● Bovine serum albumin (BSA, Sigma-Aldrich) 10 mg/mL q.s. 10 mL in H_2O; aliquots of 200 µL.

● Dithiothreitol (DTT) 6.4 mM q.s. 20 mL; MM = 154.25 g/mol, 19.74 mg in 20 mL H_2O; prepare aliquots of 500 µL. Storage at -80°C is even better.

● Sodium acetate 10 mM/Triton X-100 1% solution: add sodium acetate 10 mM q.s. 100 mL (82.03 mg acetate-Na (82.03 g/mol) in 100 mL H_2O, 1 mL Triton X-100; adjust to pH 5.6 with a few drops of acetic acid and NaOH. Aliquots of 2 mL can be prepared.

3. Preparation of noncommercial N-myristoyl protein or CoA derivatives

3.1 Myristoyl-CoA and any unusual CoA acyl derivatives

This method was first established in the early 1990s (Devadas et al., 1992; Kishore et al., 1991). It involves acyl-CoA synthetase (ACS, **Fig. 1B**0.03 U/µL final concentration in a 100 µL final volume consisting of 160 µM fatty acid or a myristate derivative (radiolabeled or clickable), 1 mM CoA (from stock 5 mM), 5 mM ATP (from stock 20 mM), 3 mM DTT, 0.05 % Triton X-100, 5 mM Tris pH 7.4, 2.5 mM $MgCl_2$, and 50 µM EGTA.

The enzyme catalyst (ACS, 0.03 U/µL final) is added to start the reaction for 1 h at 37°C. After 25 min, more than 50% of the myristate is already converted into myristoyl-CoA. This is sufficient for further labeling of protein targets. The reaction product can be used as is and without further purification in protein labeling experiments (see below).

● Radioactive labeling may also be useful for imaging and band quantification of cell extracts following pulse labeling with myristate. Radioactive imaging needs very long exposure times (Berthiaume, Peseckis, & Resh, 1995). Click chemistry-based imaging using reactive precursors may provide similar but faster results, although absolute quantification is less convenient and reliable (see §4.4).

● Chemical synthesis of the azido derivative of Myristoyl-CoA (ω-Azido undecanoic acid CoA thioester) has been described (Heal, Wickramasinghe, Leatherbarrow, & Tate, 2008). The protocol can be applied to a variety of myristate analogs which organic synthesis methods are also available (Devadas et al., 1992).

3.2 Myristoylated protein substrates

3.2.1 Fatty acid tagging of target proteins with NMT in vitro

The protocol originates from that previously set up for the myristoylation of two small GTPases, *A. thaliana* ARA6 (Boisson & Meinnel, 2003) and human ARF6 (Padovani,

Zeghouf, Traverso, Giglione, & Cherfils, 2013). The purification of ARF6 from pET21-Arf6-His6 to homogeneity is detailed in (Padovani et al., 2013).

● The final reaction volume is 1 mL with 25 µM of protein of interest, 1 µM HsNMT1, and 80 µM myristoyl-CoA. The CoA donor can correspond to any fatty acyl derivative, such as those reported in §3.1 and originating from the labeling reaction described in this section. The reaction is run for 30 min at 30°C in 50 mM Tris pH 8.0, 1 mM $MgCl_2$, 0.2 mM EGTA, and 0.3 mM DTT. In the case of small G-proteins, addition of GTP (0.2 mM) has been shown to stimulate acylation rates comparable to GDP. ScNMT is less efficient than HsNMT1 or AtNMT.

● The final product can be characterized by denaturing PAGE or mass spectrometry (see below, **Fig. 2** and **Fig. 3**)

● Use of click-reactive myristoyl-CoA can be a way to tag the protein and characterize it on gels using, for instance, DBCO- or azido-TAMRA (see below).

3.2.2 Myristoyl tagging in cell free translation systems

Insect cell-free protein synthesis from extracts of the *Spodoptera frugiperda* Sf21 cell line is an alternative to produce and tag the target protein considered *in vitro* (Suzuki et al., 2010). Coupled transcription and translation of any cDNA of interest cloned in a plasmid under the control of the T_7 promoter can be achieved with the TnT T7 Insect Cell Extract Protein Expression System (Promega, L1101). Radiolabeled or clickable myristate can be added to the reaction to follow protein myristoylation of the target by SfNMT (see §4.4).

Rabbit reticulocyte lysates (Promega, L4970) or wheat germ extracts (Promega, L4380) may be used to take advantage of mammalian or plant NMT tagging (Deichaite, Casson, Ling, & Resh, 1988; Yamauchi et al., 2010). *In vitro* transcribed mRNAs need to be produced first and provided as translation templates (Utsumi et al., 2004).

3.2.3 Bacteria-driven target labeling

Like eukaryotes, bacteria express a methionine aminopeptidase (Giglione et al., 2004; Giglione, Fieulaine, & Meinnel, 2009). Nevertheless, bacteria do not possess a myristoylation system equivalent to NMT, preventing genuine Gly-myristoylation (Deichaite et al., 1988; Giglione & Meinnel, 2022; Knoll, Johnson, Bryant, & Gordon, 1995; Rudnick, Mcwherter, Gokel, & Gordon, 1993). To allow target acylation in bacteria, one needs to (i) rely on heterologous NMT expression and (ii) take advantage of the fact that prokaryotes possess both a fatty acid import system (*fadL*) and ACS (*fadD* in *E. coli*, **Fig. 1B**). This allows bacteria to import fatty acids from the growth medium and to transform them into acyl-CoA derivatives (Giglione & Meinnel, 2022). Provided non-minimal cell extracts are added to the growth medium - usually yeast extracts - myristoyl-CoA can therefore be made available in bacterial cells for protein N-myristoylation by NMT. Nevertheless, without further supplementation, bioavailable concentrations of free myristoyl-CoA are extremely low in bacteria, because C14 derivatives are very poorly represented in yeast and because acyl compounds are weakly soluble in the absence of albumin, the natural scavenger of fatty acids in animal fluids (Giglione & Meinnel, 2022). To promote significant myristoyl-CoA concentrations, myristate - diluted from a 100-fold stock solution - can be supplied to bacteria prior to induction with IPTG at a final concentration of 50 µM bound to 6 µM BSA (Franco, Chardin, Chabre, & Paris, 1995). BSA has an average of seven myristate-binding sites (Giglione & Meinnel, 2022).

Myristoylation of any favorite target in bacteria is therefore feasible provided (i) the recombinant target gene is available and can be retrieved in the soluble fraction in, for example, *E. coli* cells; (ii) the NMT gene can be co-expressed with the target, for instance through either a compatible or a dual expression plasmid such as pETDuet-1 (Glück, Hoffmann, Koenig, & Willbold, 2010); and (iii) myristate or any derivative - including radioactive or clickable

389 compounds - is provided in the bacterial growth medium. This system was described early on
390 using ScNMT and a recombinant murine protein kinase (Duronio et al., 1990). ScNMT is
391 usually provided – for instance through the pBB131 plasmid – but appears less efficient than
392 mammalian or plant NMTs. Complete Gly-myristoylation of HIV-1 Nef protein can be
393 obtained with HsNMT1 (Glück et al., 2010).

394 Finally, having in hand a target gene easily purifiable by, for example, taking advantage
395 of a C-terminal tag - such as ARF6-His in section 2.2.1 - is of benefit to further studies but it
396 is not mandatory when studying issues related to acylation occurrence. The availability of
397 specific antibodies and/or metabolic labeling with radioactive or clickable precursors is
398 sufficient to conclude using approaches such as those described in the next section. Such
399 investigations with ARF1 and ARF6 are described in volume 404 of this series (Ha, Thomas,
400 Stauffer, & Randazzo, 2005).

401 *3.2.4 Quality controls*

402 ● Denaturing gel electrophoresis is one first gross approach. It was noted early on that protein
403 acylation often promotes faster migration of the acylated product assessed by denaturing gel
404 electrophoresis (SDS-PAGE), for example for the yeast ADP-ribosylation factors ARF1/2
405 (Lodge et al., 1997) or human ARF6 (**Fig. 2A**). Therefore, comparison of the relative intensities
406 produced data on the acylation reaction yield. However, such faster migration is not universal
407 but only occurs more frequently than average, and it is not specific since it can sometimes be
408 reversed or absent for other proteins. Longer migration times on high-resolution gels may
409 improve the migration shift between the two species (**Fig. 2B,** lane 1). If a radioactive
410 derivative is used as the CoA donor, an autoradiogram is used to directly visualize the labeling.
411 If using a clickable fatty acyl donor (reaction conditions and details are provided in §4.4),
412 reactivity with any convenient fluorophore such as TAMRA coupled to an alkyl or azide

reactive group for Cu(I)-catalyzed azide-alkyne click chemistry reactions (CuAAC) or strain-promoted azide-alkyne click chemistry reactions (SPAAC) is most useful, and fluorescence overlapping with the blue staining may be a convenient tool for checking acylation (see **Fig. 2C**). The sample is separated by SDS-PAGE and the gel directly imaged on a fluorescence imager. However, this approach is qualitative.

● MALDI-TOF/TOF characterization of the purified product is a finer assessment of protein myristoylation (see **Fig. 3A-B**) but it may be unsuitable for very large proteins (see §4.2).

4. Characterization of NMT-induced modifications on protein targets

4.1 General considerations

The rules of NMT-mediated Gly-myristoylation specificity have been investigated for decades, and it occurs in about 2% of the human and *A. thaliana* (a dicot model plant) proteomes (Castrec et al., 2018; Meinnel, 2022; Meinnel et al., 2020). Specificity was first studied in detail for the yeast enzyme ScNMT (Bhatnagar, Ashrafi, Futterer, Waksman, & Gordon, 2001; Towler, Gordon, Adams, & Glaser, 1988), which has similar specificity to other NMTs but appears to disfavor some proteins with negatively charged residues located at positions 8-9. Whether NMTs follow different rules in other organisms, including unicellular organisms, is unknown. Nevertheless, studies on organisms such *Toxoplasma gondii*, *Plasmodium falciparum*, or *Leishmania donovani* indicate similar overall rules (Brannigan et al., 2010; Broncel et al., 2020; Traverso et al., 2013a). Lys-myristoylation catalyzed by NMT appears to act only as a post-translational modification of proteins starting with Gly-Lys residues, including ARF6 (Rivière et al., 2022).

Studies aiming to define the full set of proteins targeted by NMT led to the application of proteome-wide approaches with click chemistry tools together with state-of-the-art electrospray ionization (ESI) mass spectrometry instruments. Detailed protocols and methods

have recently become available (Kallemeijn et al., 2021). Bioinformatics analyses based on machine learning approaches on partial datasets, such as using support vector machines, are also helping to complete the picture (Castrec et al., 2018; Madeo, Savojardo, Martelli, & Casadio, 2022).

This section describes several methods focusing on *in vitro* approaches with selected targets of interest, including full-length proteins or N-terminal-derived short peptides. 80% of target proteins in the complete human proteome (Meinnel, 2022), plants, and probably any organism are soluble cytosolic proteins of average length less than 40 kDa. This makes overexpression and further purification from bacterial cells to homogeneity in sufficient quantities for further studies including MS easy. With short peptides, the MS approach is often most useful for deciphering the actual modification state, including the type of modification. This can be difficult to establish, especially for proteins starting with Gly-Lys residues – both amino groups are potentially acylated - such as for ARF6. In some cases, and with longer peptides or full-length putative target proteins, additional approaches are needed. We also introduce in this context the IpaJ pipeline (**Fig. 3**; (Rivière et al., 2022)) and click chemistry-based approaches.

4.2 MALDI mass spectrometry

4.2.1 Main outlines

● 300 µL of a mixture containing 50 mM Tris (pH 8.0), 0.193 mM EGTA, 1 mM $MgCl_2$, 1 mM DTT, 5 µM sodium cholate, 40 µM Myr-CoA solution (stock solution 0.2 mM Myr-CoA, 10 mM sodium acetate, 2.5 µM sodium cholate), 0.5 µM NMT, and 100 µM of synthetic peptide or full-length protein are pre-incubated at 30°C. The myristoylation reaction is followed over time by collecting 10 µL samples further diluted in 90 µL of water/acetonitrile (90/10) solution.

461 ● The different samples are then diluted five times in the matrix solution of 5 mg/mL (i) α-
462 cyano-4-hydroxycinnamic acid solubilized in water/acetonitrile/formic acid (50/50/0.1%) for
463 peptides or (ii) 3,5-dimethoxy-4-hydroxycinnamic acid in water/acetonitrile/formic acid
464 (50/50/0.1%) for whole proteins.
465 ● 1 µL of each dilution is spotted on a metal target and dried.
466 ● MS and MS/MS spectra from each sample are acquired with a MALDI-TOF/TOF instrument
467 in positive ion mode.
468 ● Survey scans are performed using delayed extraction (390 ns) in reflector mode for a total of
469 15,000 shots. MS/MS scans are operated with a collision energy of 1 kV. Peptide and fragment
470 mass tolerances are set at 10 ppm and 0.8 Da, respectively.
471 ● Mass spectra are analyzed with PeakView 1.2 software (AB Sciex LLC). The default
472 threshold in MS/MS peak labeling and finding is 5% and centroid height percentage is 50%,
473 as recommended by the manufacturer. MS/MS deviations from theoretical values are on
474 average less than 0.03 Da.

475 *4.2.2 Notes*

476 ● For MALDI mass spectrometry, Triton X-100 needs to be avoided as a detergent. The
477 steroid-based anionic detergent sodium cholate substitutes for the Triton X-100 used in enzyme
478 kinetics studies.
479 ● MS/MS analysis allowing accurate analysis of the modification state can be achieved on
480 short peptides. Assignments of peptides with non-natural amino acids can also be performed
481 using ProteinProspector v6.2.2 (https://prospector.ucsf.edu/prospector/mshome.htm)
482 (Chalkley, Baker, Medzihradszky, Lynn, & Burlingame, 2008). Theoretical mass values of all
483 fragments are double-checked at https://web.expasy.org/peptide_mass/.

● Demonstration of Gly-myristoylation analysis of tryptic fragments from full-length proteins is feasible by MALDI MS/MS (Suzuki et al., 2006; Suzuki et al., 2010).

● MALDI MS on proteins larger than 30 kDa is challenging. In this case, electrospray ionization (ESI) MS is better suited.

● MALDI promotes one singly charged ion, usually H^+ ($[M+H]^+$), but also sometimes doubly charged ions, triply charged ions, and Na^+ adducts (+23 Da). Due to multiple charge values for each molecular mass induced by ESI, mass spectra must be deconvoluted (Xu et al., 2018).

● MALDI MS also works fine with short peptides (see an example in Figure 2, Chapter 26, this volume (Rivière, Monassa, Giglione, & Meinnel, 2023) and (Rivière et al., 2022)).

● Controls in the absence of myristoyl-CoA or catalysts such as NMT need to be run and analyzed by MS in parallel.

● The monoisotopic mass is used as a mass reference with highly pure, chemically-synthesized peptides. With purified proteins, the average mass is taken into account. The mass at the top of the mass peak is always considered.

● With high molecular weight proteins such as ARF6-His, determination of the average mass by MALDI is more accurate by taking the m/z=2 state charge into account, even though less intense and not always available (**Fig. 3**).

● Standard deviation values are obtained after several independent measurements of the mass of the same sample.

4.3 The NMT/IpaJ pipeline

This semi-quantitative assay was established to decipher the type of NMT-catalyzed modification, e.g., Gly- or Lys-myristoylation (Rivière et al., 2022). The complete pipeline - based on the high selectivity of IpaJ for myristoyl-glycine-starting proteins - is described in

detail in **Fig. 3** for a full-length protein (ARF6) but can be equally applied to short peptides, as reported (Rivière et al., 2022).

● The peptide (100 µM) is first incubated for 1 h in the presence of 0.5-1 µM HsNMT1 or HsNMT2 (T1). The buffer is the same as for NMT activity measurements but contains 5 µM cholate instead of Triton X-100.

● Full IpaJ cleavage conditions involve further incubation at 20°C for 1 h in the presence of 10 µM IpaJ-3M and 0.1 mM DTT (T2).

● 1-5 µM HsNMT1 is finally added for another 1 h at 30°C to ensure full acylation of all possible substrates (T3). T0 corresponds to the T3 timepoint (3 h) with the peptide diluted in the incubation buffer but in the absence of any enzyme.

4.4 Click chemistry-based protein imaging

4.4.1 Overview

Click chemistry approaches can be achieved if the target protein has previously been tagged with a reactive acyl myristate *in vitro*. This is detailed in §3.2.

An alternative to such *in vitro* analysis is often required to obtain *in cellulo*-relevant information on the actual myristoylation state of the target protein. This requires prior cell labeling with a myristate precursor and applies to proteins expressed in cell-free (see §3.2.2), bacterial (see §3.2.3) or mammalian cells systems (see §4.4.2). This precursor is metabolized into a CoA derivative, which NMT can then use to acylate proteins (see details in (Giglione & Meinnel, 2022)). To identify the tagged protein originating from *in cellulo* studies, it can be either immunoprecipitated with another C-terminal tag if a transgene is used or with specific - preferentially polyclonal - antibodies. In any case, PAGE analysis followed by specific imaging is often used to detect the target protein. This requires a click or biorthogonal compatible fluorophore such as alkyne- or DBCO-TAMRA derivatives, depending on the myristate label

chosen as the precursor for protein labeling. One major challenge is to ensure that the fluorescent signal arises from the selected target if not purified beforehand by immunoprecipitation. Assessing the correlation between migration and labeling is one approach to ensure this but is only indicative of the actual modification state.

If myristate reactivity is first challenged with a biotin derivative (see §2.4.3), identification of the merged fluorescence originating from a mixture of (i) a fluorescent-streptavidin probe (e.g., labeled with a Cy3 fluorophore) and (ii) the specific antibody revealed with a secondary antibody conjugated to a compatible fluorophore (see §2.4, e.g., Cy5) on the same immunoblot may be more accurate (see Figure 2 in (Neopane et al., 2022)). However, the associated data, even with unambiguous merging of fluorescent signals, does not definitively prove the myristoylation state. Therefore, to assess this *in vivo* myristoylation, specific NMT inhibitors such as IMP-1088 or DDD85646 can be used (2 µM) to demonstrate block of the modification (Kosciuk et al., 2020; Mousnier et al., 2018). An additional very strong proof may be possible by comparing overexpressing and control samples, i.e., increased intensity of the signal observed upon overexpression of the target protein. **Fig. 2D** illustrates this approach with ARF6 in human cells.

4.4.2 In cellulo labeling procedures with acyl precursors

● HEK293 cells are maintained at 37°C in 5% CO_2 in Dulbecco's modified Eagle medium (DMEM) supplemented with 10% heat-inactivated fetal calf serum, 100 U/mL penicillin (Gibco), 100 U/mL streptomycin sulfate, 2 mM L-glutamine, and a cocktail of non-essential amino acids.

● Cells are transfected with the pJAF211 plasmid in Lipofectamine 3000 (Thermo Fisher Scientific) according to the manufacturer’s instructions to express ARF6-Flag. After 3 hours of transfection, the medium is renewed with fresh culture medium, to which 20-40 µM alkyne

555 myristate (Alk-myristate) or unmodified myristate is added. After 18 to 24 h of culture, the
556 cells are harvested and lysed with a lysis buffer (PBS pH 7.4, 0.1% SDS, and 1% Triton X-
557 100) and a protease inhibitor cocktail (cOmplete ULTRA Tablets, Mini, EDTA-free,
558 EASYpack). Protein concentration is determined with the standard Bradford assay (Bio-Rad).

559 *4.4.3 In-gel imaging*

560 ● Cell lysates are diluted to 2 µg/µL total protein in lysis buffer. A mix of click reagent is
561 prepared and added to the lysates to obtain the following final concentrations: 40 µg total
562 protein, 100 µM azide probe (TAMRA and/or biotin); 1 mM $CuSO_4$; 1 mM TCEP (tris(2-
563 carboxyethyl)phosphine); and 100 µM THPTA (tris(3-hydroxypropyltriazolylmethyl)amine).
564 After 1 h of incubation at room temperature (21°C) with shaking at 12 Hz, the reaction is
565 stopped by adding EDTA to 5 mM final concentration.
566 ● For direct fluorescence analysis following SDS-PAGE when the reactive probe is coupled to
567 a TAMRA fluorophore, the products of the click reaction are denatured and diluted with 1/4
568 volume of 4x Laemmli buffer and then migrated on 12% SDS-PAGE. The metabolically
569 labeled proteins are visualized on the gels with an imager using Cy3 filters (λ_{ex}=532 nm;
570 λ_{em}=610 nm).
571 ● N-terminal protein lipidations in cell extracts mostly lead to two types of acylations,
572 myristoylation (C14) and palmitoylation (C16). These modification differ by the nature of their
573 linkage to the protein, amide or ester, respectively. Distinction between the two types of
574 modifications may be challenging because of metabolic interconversions of fatty acid
575 precursors (Giglione & Meinnel, 2022). The high susceptibility and effective cleavage of the
576 ester bond in alkaline conditions - obtained for instance with KOH (0.1 M in methanol) for 4
577 h at room temperature (Bizzozero, 1995) - is a relevant approach to check that the detected
578 acylation does arise from N-terminal amidation and is most likely catalyzed by NMT.

4.4.4 Immunoprecipitation

● One milligram of total protein from cell lysates is combined with 5 µg of target antibody and adjusted to 500 µL in IP-MS Cell Lysis Buffer (Pierce MS-compatible Magnetic IP Kit, Thermo Fisher Scientific) and then incubated overnight with shaking. The remaining procedure is carried out according to the manufacturer's protocol. In brief, 0.25 mg of magnetic beads coated with A/G proteins are washed in the lysis buffer and then incubated with the antibody/antigen mixture for 1 h at room temperature. The mixture is then washed 5 times and the antigens eluted, and the supernatant recovered and dried in a concentrator under vacuum (SpeedVac).

● Immunoprecipitation is carried out using the µMACS™ DYKDDDDK Isolation Kit (Miltenyi Biotec) according to the manufacturer's protocol.

● The tagged protein is visualized with specific antibodies. An example of ARF6 detection with Flag-tag antibodies is shown in **Fig. 2E**.

● To increase the concentration, protein samples can be subjected to methanol:chloroform (4:1) precipitation and centrifuged for 5 min at 13,000 x *g*. The upper aqueous phase is discarded to leave the interface layer containing intact protein precipitate. 450 µL methanol is added to the tube, vortexed, and centrifuged for 5 min at 13,000 x *g* to pellet the protein. The pellet is washed with 450 µL methanol to remove residual reaction components. The pellets are allowed to air dry. The dried protein precipitates can be resolubilized in Laemmli sample buffer for further SDS-PAGE analysis.

4.4.5 Fluorescence imaging after immunoblotting

● Proteins separated by 12-15% SDS-PAGE are transferred (25 mM Tris; 190 mM glycine; 20% MetOH) onto a polyvinylidene fluoride (PVDF) membrane at 4°C 30 V overnight. The

PVDF membrane is incubated and blocked in 3% TBST BSA (20 mM Tris pH 7.5; 150 mM NaCl; 0.1% Tween 20; 3% BSA) for 90 min at room temperature.

● The membrane is incubated with the primary – here anti-Flag or anti-ARF6 - antibody diluted 1:1000 according to the manufacturer's recommendations, before being washed 5 times in TBST BSA 1%.

● The membrane is incubated with a secondary anti-IgG conjugate antibody tagged with a Cy5 fluorophore and the streptavidin–Cy3 derivative diluted at 1:10,000 in the blocking buffer at 4°C overnight.

● Imaging is performed with both the Cy3 and Cy5 channels and the fluorescence merged as required.

5. Structural studies of NMT and its complexes with substrates and products

5.1 Structural overview

NMTs are made up of a two-GNAT core (Meinnel et al., 2020). The N-terminal domain is of varying length and is not folded. High resolution crystal structures are available for NMTs from *Aspergillus fumigatus* (Shimada, Suzuki, & Katakura, 2015), *Candida albicans* (Bhatnagar et al., 1998), *Homo sapiens* (both forms and various isoforms (Castrec et al., 2018; Thinon et al., 2014)), *Leishmania donovani* and *major* (Brannigan et al., 2010; Frearson et al., 2010), *Plasmodium vivax* (Goncalves et al., 2012) and *Saccharomyces cerevisiae* (Wu et al., 2007). HsNMT1's longest structures start at residue 99, which includes a crucial B'A' helix (Castrec et al., 2018). Many HsNMT1 structures start at residue 109 or 116. HsNMT2 crystal structures start at residues 112 (4C2X, (Thinon et al., 2014)) and 116 (6PAU (Kosciuk et al., 2020)) and miss the important element involved in a major conformational change contributing to product release (Dian et al., 2020).

AlphaFold software predictions (Jumper et al., 2021) of the structure of several NMTs are available at UniProt (https://www.uniprot.org/). Interestingly, the AlphaFold predictions of HsNMT, PvNMT and AtNMT structures suggest that there is an additional alpha helix at the beginning of the folded GNAT domain (residues Asn82 in HsNMT1, Met88 in HsNMT2, Asp27 in PvNMT, Leu31 in AtNMT1), a structure hitherto not identified by crystallographic approaches (**Fig. 4A** for both HsNMTA and HsNMT2; see also AF-Q9LTR9-F1 and AF-A0A1G4HIY1-F1 for AtNMT1 and PvNMT at https://alphafold.com/).

Recent investigations have provided details of NMTs in action with their two substrates. Below are the approaches used to capture such short-lived complexes.

5.2 Crystallization and structure determination

5.2.1 General crystallization conditions

In recent studies, HsNMT1(*s*) was used to solve the structures of the complexes with various substrate peptides (Castrec et al., 2018; Dian et al., 2020; Kosciuk et al., 2020; Rivière et al., 2022). The associated PDB entries are indicated in the published papers.

Suitable crystals of HsNMT1:MyrCoA:peptide substrates were obtained by co-crystallization using the hanging-drop vapor diffusion method at 20°C in the crystallization conditions previously described (Castrec et al., 2018; Dian et al., 2020). Briefly, crystallization droplets are formed by mixing 2 µL of the of HsNMT1:MyrCoA:peptide complex (ratio 1:1.5:1.5) at 6-9 mg/mL with 2 µL of the precipitant solution containing either 0.1 M $MgCl_2$, 0.2 M NaCl, 0.1 M sodium citrate pH 5.6, and 18-24% (w/v) PEG 6K or 0.1 M sodium acetate pH 4.6 and 18-24% (w/v) PEG 6K. Crystals are cryoprotected in the reservoir solution supplemented with 15% (v/v) glycerol and flash cooled in liquid nitrogen.

5.2.2 Obtaining crystals of NMT in complex with reactants or reaction intermediates

GNATs use a sequential ordered Bi-Bi mechanism involving binding first to the CoA derivative and then to the peptidyl target (Salah Ud-Din, Tikhomirova, & Roujeinikova, 2016). This also applies to NMTs and has been demonstrated for ScNMT and HsNMT1 (Rocque, Mcwherter, Wood, & Gordon, 1993; Rudnick et al., 1991). This feature needs to be taken into account in crystallographic trials.

● CoA derivative complexes. NMT crystal structures – as is the case for most GNATs – are most often determined in complex with their cognate CoA derivative. Crystals devoid of the CoA derivative are rarely obtained. This probably originates from the structural remodeling of the CoA binding site upon binding. When overexpressed in *E. coli*, the acetyl-CoA derivative tightly binds to GNATs and it appears unnecessary to add it. Nevertheless, myristoyl-CoA is not available, as fatty acyl CoA derivatives do not accumulate in *E. coli* (Giglione & Meinnel, 2022; Meinnel, 2022). The growth medium can be supplemented with myristate, as it can be converted *in cellulo* by ACS in bacteria (**Fig. 1B**). Myristoyl-CoA can also be added in crystallization trials.

● Peptidyl complexes. Multiple factors have significant impact on the success in obtaining crystals of intermediates. From our experience gained while generating the data reported in (Dian et al., 2020) with peptides X (GNCSFSKRRA), Y (GSNKSKPK), U (*ac*-GKSFSKPR), and V (*ac*-KSFSKPR), these include:

- Soaking (peptide Y) instead of co-crystallization (peptide X) to reduce reaction time. It is tempting to say that a 15 min soak used to solve the complex with peptide Y seems to have been sufficient to pick up the intermediate, while co-crystallization with peptide X gave time for the reaction to occur;

- Both low and different pHs of the precipitant solutions (pH 4.6 with peptide Y and pH 5.6 with peptide X, (Dian et al., 2020)) significantly contributed to slowing down the NMT reaction (optimum pH is 8.0);

- Nature of the two peptides for which NMT displays different catalytic efficiencies;
- Crystal trials must be performed under many different conditions (i.e., different peptides, different peptide concentrations, different soaking times), and most of them will remain inconclusive (e.g., no crystal, poor resolution, no intermediate). Only successful datasets are presented in publications, probably representing the outcome of many trials. We also observed that several crystals need to be collected from the same batch to finally observe a few of them showing reaction intermediates.

5.2.3 Dataset collection, structure resolution, and refinement

Complete X-ray datasets of complexes are collected at 100*K*, a single wavelength from a single crystal, at synchrotron facilities such as the French National Synchrotron Facility (SOLEIL) PROXIMA-1 or PROXIMA-2 beamlines or at the European Radiation Synchrotron Facility (ESRF) with the ID30A1 and ID30A3 beamlines.

● Datasets are integrated with XDS (Kabsch, 1993) and scaled and reduced using AIMLESS from the CCP4 package (Evans & Murshudov, 2013). For crystals suffering from anisotropic diffraction, data are processed with STARANISO on unmerged data (Tickle et al., 2018) before AIMLESS data reduction.

● Crystals of HsNMT1 complexes belong essentially to the space group $P2_12_12$ with similar unit cell parameters, except for some belonging to C2 with distinct unit cell parameters. In both space groups identified, unit cells contain two NMT molecules per asymmetric unit. Structure resolution was accomplished in all cases using the molecular replacement method and solved using PHASER (Mccoy et al., 2007) and the HsNMT1:MyrCoA:peptide ternary complex (PDB entry 5O9T or 6SK2) as a search model. The structure of AN was solved using MOLREP (Vagin & Teplyakov, 1997) and protein coordinates of HsNMT1:MyrCoA (PDB entry 5O9T) as a search model.

● Structures are subjected to alternating refinement cycles using PHENIX and manual model building using COOT (Adams et al., 2010; Emsley, Lohkamp, Scott, & Cowtan, 2010; Murshudov et al., 2011). Good quality electron density maps enable the refinement of substrate peptide, reaction intermediate, and reaction product molecules bound to HsNMT1 in each complex. Chemical compound libraries are generated using the PRODRG server (Schuttelkopf & Van Aalten, 2004) in combination with eLBOW from the PHENIX suite. The geometry of the final models is validated using MOLPROBITY (Chen et al., 2010). Figures are generated using PYMOL (DeLano Scientific LLC, http://pymol.sourceforge.net/).

● Omit electron density maps can be calculated using PolderMap (Liebschner et al., 2017) from the Phenix suite after omitting the peptide of each active site and excluding the bulk solvent around the omitted region (**Fig. 4B**).

● Ball and stick representations in 2D are a good way to challenge and compare active site interactions (**Fig. 4C**)

6. Conclusions and future prospects

Here we report a series of multiscale biochemical analyses that allow the capture and fine definition of NMT catalysis and the validation of putative targets. This permits not only time and space investigation but also challenging substrate selectivity experiments based on the chemical choice and specificity provided by this unique family of catalysts. This exemplifies the remarkable fluidity of the reaction catalyzed *in vitro* by NMTs. Other - mostly click chemistry-based - methods are available for fine characterization of myristoylation at the cellular proteome level (see Chapter 24 by H. Lin et al. in this volume or (Kallemeijn et al., 2021)). Kinetic analysis of myristoylation by NMTs of octapeptides derived from actual protein N-termini have been validated as a relevant and robust approach to contribute to completing this effort at proteome scales (Boisson, Giglione, & Meinnel, 2003; Castrec et al.,

2018; Meinnel, 2022; Traverso et al., 2013a). Such methods are detailed in Chapter 26 in this volume (Rivière et al., 2023).

Future progress in biochemical characterization will need to better address the acylation yield (i.e., the ratio of each N-terminal acylation state to the total amount of a given protein) of each target, as it likely varies from one physiological condition to another. With differences in myristoylation, the overall subcellular localization of the same target changes and most likely favors different functions of the target. Therefore, investigation of the myristoylation yield on a maximum number of targets - preferentially not overproduced *in cellulo* – will be required in the future. Although such approaches exist in the case of N-terminal acetylation (Bienvenut, Giglione, & Meinnel, 2015, 2017; Bogaert & Gevaert, 2020), this is not yet available for NMT targets. This approach will probably need to enrich the N-terminal peptides without loss of the most hydrophobic ones, including N-myristoylated peptides. Unfortunately, currently available click-based approaches are not directly suited to this purpose, as they lead to the selection of only the myristoylated state and the loss of all other isoforms.

Acknowledgements

We thank the I2BC proteomic platform SICaPS for productive and collaborative interactions over the past decade. We thank the French National Synchrotron Facility (SOLEIL) for providing the synchrotron radiation facilities and the staff of the PROXIMA-1 & -2 beamlines and the European Synchrotron Radiation Facility (ESRF) staff for help with data collection. We acknowledge David Cornu, Flaria El Khoury, Lucile Jomat, Jean-Pierre Le Caer, Virginie Redeker, and Laila Sago for their respective inputs in the setting of the various approaches presented in this manuscript.

Funding

This work was supported by French National Research Agency (ANR) DynaMYT (ANR-20-CE44-0013) and Fondation ARC (ARCPJA32020060002137) grants to TM. This work has benefited from the support from a French State grant (Saclay Plant Sciences, reference n° ANR-17-EUR-0007, EUR SPS-GSR) under a France 2030 program (reference n° ANR-11-IDEX-0003), from the I2BC crystallization platform supported by FRISBI (ANR-10-INSB-05-01), and from the facilities and expertise of the I2BC proteomic platform SICaPS, supported by IBiSA, Ile de France Region, Plan Cancer, CNRS and Paris-Sud University. FR was supported by grants from Région Ile-de-France (17012695) and Fondation pour la Recherche Médicale (FDT202001010779).

References

Adams, P. D., Afonine, P. V., Bunkoczi, G., Chen, V. B., Davis, I. W., Echols, N., et al. (2010). PHENIX: a comprehensive Python-based system for macromolecular structure solution. *Acta Crystallographica Section D, 66*, 213-221.

Berthiaume, L., Peseckis, S. M., & Resh, M. D. (1995). Synthesis and use of iodo-fatty acid analogs. *Methods in Enzymology, 250*, 454-466.

Bhatnagar, R. S., Ashrafi, K., Futterer, K., Waksman, G., & Gordon, J. I. (2001). Biology and enzymology of protein N-myristoylation. In F. Tamanoi & D. S. Sigman (Eds.), *The Enzymes* (Vol. XXI (Protein lipidation), pp. 241-286). San Diego: Academic Press.

Bhatnagar, R. S., Futterer, K., Farazi, T. A., Korolev, S., Murray, C. L., Jackson-Machelski, E., et al. (1998). Structure of N-myristoyltransferase with bound myristoylCoA and peptide substrate analogs. *Nature Structural Biology, 5*, 1091-1097.

Bienvenut, W. V., Giglione, C., & Meinnel, T. (2015). Proteome-wide analysis of the amino terminal status of Escherichia coli proteins at the steady-state and upon deformylation inhibition. *Proteomics, 15*, 2503-2518.

772 Bienvenut, W. V., Giglione, C., & Meinnel, T. (2017). SILProNAQ: a convenient approach for
773 proteome-wide analysis of protein N-termini and N-terminal acetylation quantitation.
774 *Methods in Molecular Biology, 1574*, 17-34.
775 Bizzozero, O. A. (1995). Chemical analysis of acylation sites and species. *Methods in*
776 *Enzymology, 250*, 361-379.
777 Bogaert, A., & Gevaert, K. (2020). Protein amino-termini and how to identify them. *Expert*
778 *Review of Proteomics, 17*, 581-594.
779 Boisson, B., Giglione, C., & Meinnel, T. (2003). Unexpected protein families including cell
780 defense components feature in the N-myristoylome of a higher eukaryote. *Journal of*
781 *Biological Chemistry, 278*, 43418-43429.
782 Boisson, B., & Meinnel, T. (2003). A continuous assay of myristoyl-CoA:protein N-
783 myristoyltransferase for proteomic analysis. *Analytical Biochemistry, 322*, 116-123.
784 Bradford, M. M. (1976). A rapid and sensitive method for the quantitation of microgram
785 quantities of protein utilizing the principle of protein-dye binding. *Analytical*
786 *Biochemistry, 72*, 248-254.
787 Brannigan, J. A., Smith, B. A., Yu, Z., Brzozowski, A. M., Hodgkinson, M. R., Maroof, A., et
788 al. (2010). N-myristoyltransferase from Leishmania donovani: structural and functional
789 Characterisation of a potential drug target for visceral Leishmaniasis. *Journal of*
790 *Molecular Biology, 396*, 985-999.
791 Broncel, M., Dominicus, C., Vigetti, L., Nofal, S. D., Bartlett, E. J., Touquet, B., et al. (2020).
792 Profiling of myristoylation in Toxoplasma gondii reveals an N-myristoylated protein
793 important for host cell penetration. *eLife, 9*, e57861.
794 Burnaevskiy, N., Fox, T. G., Plymire, D. A., Ertelt, J. M., Weigele, B. A., Selyunin, A. S., et
795 al. (2013). Proteolytic elimination of N-myristoyl modifications by the Shigella
796 virulence factor IpaJ. *Nature, 496*, 106-109.

797 Burnaevskiy, N., Peng, T., Reddick, L. E., Hang, H. C., & Alto, N. M. (2015). Myristoylome
798 profiling reveals a concerted mechanism of ARF GTPase deacylation by the bacterial
799 protease IpaJ. *Molecular Cell, 58*, 110-122.
800 Casey, P. J., & Buss, J. E. (1995). Lipid modifications of proteins. In P. J. Casey & J. E. Buss
801 (Eds.), *Methods in Enzymolology* (Vol. 250, pp. 754).
802 Castrec, B., Dian, C., Ciccone, S., Ebert, C. L., Bienvenut, W. V., Le Caer, J.-P., et al. (2018).
803 Structural and genomic decoding of human and plant myristoylomes reveals a
804 definitive recognition pattern. *Nature Chemical Biology, 14*, 671-679.
805 Chalkley, R. J., Baker, P. R., Medzihradszky, K. F., Lynn, A. J., & Burlingame, A. L. (2008).
806 In-depth analysis of tandem mass spectrometry data from disparate instrument types.
807 *Molecular & Cellular Proteomics, 7*, 2386-2398.
808 Chen, V. B., Arendall, W. B., 3rd, Headd, J. J., Keedy, D. A., Immormino, R. M., Kapral, G.
809 J., et al. (2010). MolProbity: all-atom structure validation for macromolecular
810 crystallography. *Acta Crystallographica Section D, 66*, 12-21.
811 Deichaite, I., Casson, L. P., Ling, H. P., & Resh, M. D. (1988). In vitro synthesis of pp60v-src:
812 myristylation in a cell-free system. *Molecular and Cellular Biology, 8*, 4295-4301.
813 Devadas, B., Lu, T., Katoh, A., Kishore, N. S., Wade, A. C., Mehta, P. P., et al. (1992).
814 Substrate specificity of Saccharomyces cerevisiae myristoyl-CoA: protein N-
815 myristoyltransferase. Analysis of fatty acid analogs containing carbonyl groups,
816 nitrogen heteroatoms, and nitrogen heterocycles in an in vitro enzyme assay and
817 subsequent identification of inhibitors of human immunodeficiency virus I replication.
818 *Journal of Biological Chemistry, 267*, 7224-7239.
819 Dian, C., Pérez-Dorado, I., Rivière, F., Asensio, T., Legrand, P., Ritzefeld, M., et al. (2020).
820 High-resolution snapshots of human N-myristoyltransferase in action illuminate a

mechanism promoting N-terminal Lys and Gly myristoylation. *Nature Communications, 11*, 1132.

Dümmler, A., Lawrence, A. M., & de Marco, A. (2005). Simplified screening for the detection of soluble fusion constructs expressed in E. coli using a modular set of vectors. *Microbial Cell Factories, 4*, 34.

Duronio, R. J., Jackson-Machelski, E., Heuckeroth, R. O., Olins, P. O., Devine, C. S., Yonemoto, W., et al. (1990). Protein N-myristoylation in Escherichia coli: reconstitution of a eukaryotic protein modification in bacteria. *Proceedings of the National Academy of Sciences, 87*, 1506-1510.

Emsley, P., Lohkamp, B., Scott, W. G., & Cowtan, K. (2010). Features and development of Coot. *Acta Crystallographica Section D, 66*, 486-501.

Enríquez-Flores, S., De la Mora-De la Mora, J. I., Flores-López, L. A., Cabrera, N., Fernández-Lainez, C., Hernández-Alcántara, G., et al. (2022). Improved yield, stability, and cleavage reaction of a novel tobacco etch virus protease mutant. *Applied Microbiology and Biotechnology, 106*, 1475-1492.

Evans, P. R., & Murshudov, G. N. (2013). How good are my data and what is the resolution? *Acta Crystallographica Section D, 69*, 1204-1214.

Franco, M., Chardin, P., Chabre, M., & Paris, S. (1995). Myristoylation of ADP-ribosylation factor 1 facilitates nucleotide exchange at physiological Mg2+ levels. *Journal of Biological Chemistry, 270*, 1337-1341.

Frearson, J. A., Brand, S., McElroy, S. P., Cleghorn, L. A., Smid, O., Stojanovski, L., et al. (2010). N-myristoyltransferase inhibitors as new leads to treat sleeping sickness. *Nature, 464*, 728-732.

844 Frottin, F., Martinez, A., Peynot, P., Mitra, S., Holz, R. C., Giglione, C., et al. (2006). The
845 proteomics of N-terminal methionine cleavage. *Molecular & Cellular Proteomics, 5*,
846 2336-2349.
847 Giglione, C., Boularot, A., & Meinnel, T. (2004). Protein N-terminal methionine excision.
848 *Cellular and Molecular Life Sciences, 61*, 1455-1474.
849 Giglione, C., Fieulaine, S., & Meinnel, T. (2009). Cotranslational processing mechanisms:
850 towards a dynamic 3D model. *Trends in Biochemical Sciences, 34*, 417-426.
851 Giglione, C., & Meinnel, T. (2022). Mapping the myristoylome through a complete
852 understanding of protein myristoylation biochemistry. *Progress in Lipid Research, 85*,
853 101139.
854 Glück, J. M., Hoffmann, S., Koenig, B. W., & Willbold, D. (2010). Single vector system for
855 efficient N-myristoylation of recombinant proteins in E. coli. *PloS One, 5*, e10081.
856 Goncalves, V., Brannigan, J. A., Whalley, D., Ansell, K. H., Saxty, B., Holder, A. A., et al.
857 (2012). Discovery of Plasmodium vivax N-myristoyltransferase inhibitors: screening,
858 synthesis, and structural characterization of their binding mode. *Journal of Medicinal*
859 *Chemistry, 55*, 3578-3582.
860 Gordon, J. I., Duronio, R. J., Rudnick, D. A., Adams, S. P., & Gokel, G. W. (1991). Protein N-
861 myristoylation. *Journal of Biological Chemistry, 266*, 8647-8650.
862 Ha, V. L., Thomas, G. M., Stauffer, S., & Randazzo, P. A. (2005). Preparation of myristoylated
863 Arf1 and Arf6. *Methods in Enzymology, 404*, 164-174.
864 Heal, W. P., Wickramasinghe, S. R., Leatherbarrow, R. J., & Tate, E. W. (2008). N-Myristoyl
865 transferase-mediated protein labelling in vivo. *Organic and Biomolecular Chemistry,*
866 *6*, 2308-2315.
867 Jumper, J., Evans, R., Pritzel, A., Green, T., Figurnov, M., Ronneberger, O., et al. (2021).
868 Highly accurate protein structure prediction with AlphaFold. *Nature, 596*, 583-589.

869 Kabsch, W. (1993). Automatic processing of rotation diffraction data from crystals of initially
870 unknown symmetry and cell constants. *Journal of Applied Crystallography, 26*, 795-
871 800.
872 Kallemeijn, W. W., Lanyon-Hogg, T., Panyain, N., Goya Grocin, A., Ciepla, P., Morales-
873 Sanfrutos, J., et al. (2021). Proteome-wide analysis of protein lipidation using chemical
874 probes: in-gel fluorescence visualization, identification and quantification of N-
875 myristoylation, N- and S-acylation, O-cholesterylation, S-farnesylation and S-
876 geranylgeranylation. *Nature Protocols, 16*, 5083-5122.
877 Kapust, R. B., Tözsér, J., Fox, J. D., Anderson, D. E., Cherry, S., Copeland, T. D., et al. (2001).
878 Tobacco etch virus protease: mechanism of autolysis and rational design of stable
879 mutants with wild-type catalytic proficiency. *Protein Engineering, Design and*
880 *Selection, 14*, 993-1000.
881 Kishore, N. S., Lu, T. B., Knoll, L. J., Katoh, A., Rudnick, D. A., Mehta, P. P., et al. (1991).
882 The substrate specificity of Saccharomyces cerevisiae myristoyl-CoA:protein N-
883 myristoyltransferase. Analysis of myristic acid analogs containing oxygen, sulfur,
884 double bonds, triple bonds, and/or an aromatic residue. *Journal of Biological*
885 *Chemistry, 266*, 8835-8855.
886 Knoll, L. J., Johnson, D. R., Bryant, M. L., & Gordon, J. I. (1995). Functional significance of
887 myristoyl moiety in N-myristoyl proteins. *Methods in Enzymology, 250*, 405-435.
888 Kosciuk, T., Price, I. R., Zhang, X., Zhu, C., Johnson, K. N., Zhang, S., et al. (2020). NMT1
889 and NMT2 are lysine myristoyltransferases regulating the ARF6 GTPase cycle. *Nature*
890 *Communications, 11*, 1067.
891 Liebschner, D., Afonine, P. V., Moriarty, N. W., Poon, B. K., Sobolev, O. V., Terwilliger, T.
892 C., et al. (2017). Polder maps: improving OMIT maps by excluding bulk solvent. *Acta*
893 *Crystallographica Section D, 73*, 148-157.

Lodge, J. K., Jackson-Machelski, E., Devadas, B., Zupec, M. E., Getman, D. P., Kishore, N., et al. (1997). N-myristoylation of Arf proteins in Candida albicans: an in vivo assay for evaluating antifungal inhibitors of myristoyl-CoA: protein N-myristoyltransferase. *Microbiology, 143*, 357-366.

Madeo, G., Savojardo, C., Martelli, P. L., & Casadio, R. (2022). SVMyr: a Web server detecting co- and post-translational myristoylation in proteins. *Journal of Molecular Biology, 434*, 167605.

Martin, D. D., Beauchamp, E., & Berthiaume, L. G. (2011). Post-translational myristoylation: Fat matters in cellular life and death. *Biochimie, 93*, 18-31.

McCoy, A. J., Grosse-Kunstleve, R. W., Adams, P. D., Winn, M. D., Storoni, L. C., & Read, R. J. (2007). Phaser crystallographic software. *Journal of Applied Crystallography, 40*, 658-674.

Meinnel, T. (2022). Comment on "Binding affinity determines substrate specificity and enables discovery of substrates for N-Myristoyltransferases". *ACS Catalysis, 12*, 8195-8201.

Meinnel, T., Dian, C., & Giglione, C. (2020). Myristoylation, an ancient protein modification mirroring eukaryogenesis and evolution. *Trends in Biochemical Sciences, 45*, 619-632.

Mousnier, A., Bell, A. S., Swieboda, D. P., Morales-Sanfrutos, J., Perez-Dorado, I., Brannigan, J. A., et al. (2018). Fragment-derived inhibitors of human N-myristoyltransferase block capsid assembly and replication of the common cold virus. *Nature Chemistry, 10*, 599-606.

Murshudov, G. N., Skubak, P., Lebedev, A. A., Pannu, N. S., Steiner, R. A., Nicholls, R. A., et al. (2011). REFMAC5 for the refinement of macromolecular crystal structures. *Acta Crystallographica Section D, 67*, 355-367.

Nautiyal, K., & Kuroda, Y. (2018). A SEP tag enhances the expression, solubility and yield of recombinant TEV protease without altering its activity. *New Biotechnology, 42*, 77-84.

Neopane, K., Kozlov, N., Negoita, F., Murray-Segal, L., Brink, R., Hoque, A., et al. (2022). Blocking AMPK β1 myristoylation enhances AMPK activity and protects mice from high-fat diet-induced obesity and hepatic steatosis. *Cell Reports, 41*, 111862.

Padovani, D., Zeghouf, M., Traverso, J. A., Giglione, C., & Cherfils, J. (2013). High yield production of myristoylated Arf6 small GTPase by recombinant N-myristoyl transferase. *Small GTPases, 4*, 3-8.

Pierre, M., Traverso, J. A., Boisson, B., Domenichini, S., Bouchez, D., Giglione, C., et al. (2007). N-Myristoylation regulates the SnRK1 pathway in Arabidopsis. *The Plant Cell, 19*, 2804-2821.

Rivière, F., Dian, C., Dutheil, R. F., Monassa, P., Giglione, C., & Meinnel, T. (2022). Structural and large-scale analysis unveil the intertwined paths promoting NMT-catalyzed lysine and glycine myristoylation. *Journal of Molecular Biology, 434*, 167843.

Rivière, F., Monassa, P., Giglione, C., & Meinnel, T. (2023). Kinetic and catalytic features of N-myristoyltransferases. *Methods in Enzymology, 686*, Chapter 26.

Rocque, W. J., McWherter, C. A., Wood, D. C., & Gordon, J. I. (1993). A comparative analysis of the kinetic mechanism and peptide substrate specificity of human and Saccharomyces cerevisiae myristoyl-CoA:protein N-myristoyltransferase. *Journal of Biological Chemistry, 268*, 9964-9971.

Rudnick, D. A., Duronio, R. J., & Gordon, J. I. (1992). Methods for studying myristoyl-coenzyme A: protein N-myristoyltransferase. In N. M. Hooper & A. J. Turner (Eds.), *Lipid modification by proteins. A practical approach* (pp. 37-61). Oxford: IRL Press.

Rudnick, D. A., McWherter, C. A., Gokel, G. W., & Gordon, J. I. (1993). MyristoylCoA:protein N-myristoyltransferase. *Advances in Enzymology and Related Areas of Molecular Biology, 67*, 375-430.

Rudnick, D. A., McWherter, C. A., Rocque, W. J., Lennon, P. J., Getman, D. P., & Gordon, J. I. (1991). Kinetic and structural evidence for a sequential ordered Bi Bi mechanism of catalysis by Saccharomyces cerevisiae myristoyl-CoA:protein N-myristoyltransferase. *Journal of Biological Chemistry, 266*, 9732-9739.

Salah Ud-Din, A. I., Tikhomirova, A., & Roujeinikova, A. (2016). Structure and functional diversity of GCN5-related N-acetyltransferases (GNAT). *International Journal of Molecular Sciences, 17*, E1018.

Schuttelkopf, A. W., & van Aalten, D. M. (2004). PRODRG: a tool for high-throughput crystallography of protein-ligand complexes. *Acta Crystallographica Section F, 60*, 1355-1363.

Shimada, T., Suzuki, M., & Katakura, S. I. (2015). Structure of N-myristoyltransferase from Aspergillus fumigatus. *Acta Crystallographica Section D, 71*, 754-761.

Suzuki, T., Ito, M., Ezure, T., Shikata, M., Ando, E., Utsumi, T., et al. (2006). N-Terminal protein modifications in an insect cell-free protein synthesis system and their identification by mass spectrometry. *Proteomics, 6*, 4486-4495.

Suzuki, T., Moriya, K., Nagatoshi, K., Ota, Y., Ezure, T., Ando, E., et al. (2010). Strategy for comprehensive identification of human N-myristoylated proteins using an insect cell-free protein synthesis system. *Proteomics, 10*, 1780-1793.

Thinon, E., Serwa, R. A., Broncel, M., Brannigan, J. A., Brassat, U., Wright, M. H., et al. (2014). Global profiling of co- and post-translationally N-myristoylated proteomes in human cells. *Nature Communications, 5*, 4919.

Tickle, I. J., Flensburg, C., Keller, P., Paciorek, W., Sharff, A., Vonrhein, C., et al. (2018). STARANISO (http://staraniso.globalphasing.org/cgi-bin/staraniso.cgi).

Towler, D. A., Gordon, J. I., Adams, S. P., & Glaser, L. (1988). The biology and enzymology of eukaryotic protein acylation. *Annual Review of Biochemistry, 57*, 69-99.

968 Traverso, J. A., Giglione, C., & Meinnel, T. (2013a). High-throughput profiling of N-
969 myristoylation substrate specificity across species including pathogens. *Proteomics, 13*,
970 25-36.
971 Traverso, J. A., Micalella, C., Martinez, A., Brown, S. C., Satiat-Jeunemaitre, B., Meinnel, T.,
972 et al. (2013b). Roles of N-Terminal fatty acid acylations in membrane compartment
973 partitioning: Arabidopsis h-type thioredoxins as a case study. *The Plant Cell, 25*, 1056-
974 1077.
975 Utsumi, T., Nakano, K., Funakoshi, T., Kayano, Y., Nakao, S., Sakurai, N., et al. (2004).
976 Vertical-scanning mutagenesis of amino acids in a model N-myristoylation motif
977 reveals the major amino-terminal sequence requirements for protein N-myristoylation.
978 *Eur J Biochem, 271*, 863-874.
979 Vagin, A., & Teplyakov, A. (1997). MOLREP: an automated program for molecular
980 replacement. *Journal of Applied Crystallography, 30*, 1022-1225.
981 Wu, J., Tao, Y., Zhang, M., Howard, M. H., Gutteridge, S., & Ding, J. (2007). Crystal structures
982 of Saccharomyces cerevisiae N-myristoyltransferase with bound myristoyl-CoA and
983 inhibitors reveal the functional roles of the N-terminal region. *Journal of Biological*
984 *Chemistry, 282*, 22185-22194.
985 Xu, G., Stupak, J., Yang, L., Hu, L., Guo, B., & Li, J. (2018). Deconvolution in mass
986 spectrometry based proteomics. *Rapid Communications in Mass Spectrometry, 32*,
987 763-774.
988 Yamauchi, S., Fusada, N., Hayashi, H., Utsumi, T., Uozumi, N., Endo, Y., et al. (2010). The
989 consensus motif for N-myristoylation of plant proteins in a wheat germ cell-free
990 translation system. *FEBS Journal, 277*, 3596-3607.
991
992

Figure Legends

Fig. 1. Reactions catalyzed by the main enzymes useful for NMT studies. (A) NMT. (B) ACS, X is any acyl chain and may possibly end with an azide or an alkyne reactive group. (C) IpaJ.

Fig. 2. Electrophoresis analysis of the myristoylation state of a protein target. ARF6-His-tag reactivity with myristate derivatives was probed by denaturing electrophoresis and revealed using different approaches. (A) 12% SDS-PAGE analysis of ARF6 after Coomassie blue staining; Lane 1, molecular weight marker; Lane 2, unmodified ARF6; Lane 3 myristoylated ARF6. Panels B &C. 15% SDS-PAGE ARF6 analysis after labeling with Myr-Alk or myristate or mixed with plant cell extracts (lanes 3-7) or not (lane 1). The PEG3-azide-TAMRA probe was reacted at increasing concentrations of 1, 10, 25, 50 and 100 μM (lanes 3-7). Lane 8 corresponds to ARF6 labeled with the unclickable physiological myristate. Lane 2 is the molecular marker. (B) Coomassie blue staining (C) TAMRA fluorescence imaging of the same gel after azide-TAMRA click reaction. The two arrows indicate the unmodified (top) and modified (bottom) versions of ARF6. Only the modified, faster migrating version reacts with the TAMRA click probe. (D) Coomassie blue (left panel) and TAMRA fluorescence after azide-TAMRA-biotin click reaction (right panel) signals of protein samples from HEK293 protein lysates (40 μg/lane) analyzed by SDS-PAGE. Cells were fed with Myr-Alk or not and ARF6-Flag was overexpressed or not, as indicated. (E) HEK293 protein lysates overproducing samples ARF6-Flag (INP, input) were immunoprecipitated (IP) and analyzed by SDS-PAGE and revealed by blue staining (left panel) or by immunoblotting with anti-Flag antibody (right panel).

Fig. 3. MALDI MS IpaJ pipeline applied to myristoylation of full-length protein ARF6. The monocharged (z=1) and doubly-charged (z=2) masses are visible on the m/z MALDI MS spectrum. The spectra displayed in the figure were obtained with HsNMT2. Similar data were obtained with HsNMT1. Masses are deduced from the more resolute doubly charged masses. (A) T0, ARF6 protein alone. (B) T1, myristoylated ARF6 (Myr-ARF6) on its N-terminal Gly. (C) T3, ARF6 devoid of N-terminal Gly as a result of IpaJ action (ΔG-ARF6) and remyristoylation of the Lys2 side chain by NMT (ΔG-Myr(K)-ARF6). (D) Recapitulation of the complete IpaJ pipeline with expected masses at each step and comparison between theoretical and measured masses.

Fig. 4. Main structural components of NMTs. (A) AlphaFold-predicted 3D structures of HsNMT1 and HsNMT2 (UniProt entries P30419 and O60551, AlphaFold IDs AF-P30419-F1 and AF-O60551-F1). Overlap of the two structures each displayed in green and pink, respectively. The additional N-terminal helix (17 residues long) is displayed on top of the panel. The structures correspond to residues 85-496 and 88-498, respectively. The disordered N-terminus is not displayed. Both Myristoyl-CoA and peptide ligands at their binding sites are figured in orange and yellow, respectively. (B) Detailed “fofc omit” sigmaA-weighted electron density maps (mFobs – DFcalc, PHIcalc) are shown in grey for each of the structures with peptide ligand *ac*-K undergoing Lys-myristoylation., Myr, MyrCoA, and CoA carbon atoms are in orange when unlinked to the peptide moiety and in green when covalently bound to the peptide. (C) Overlap of GK (HPCA) with *ac*K (A subunit).

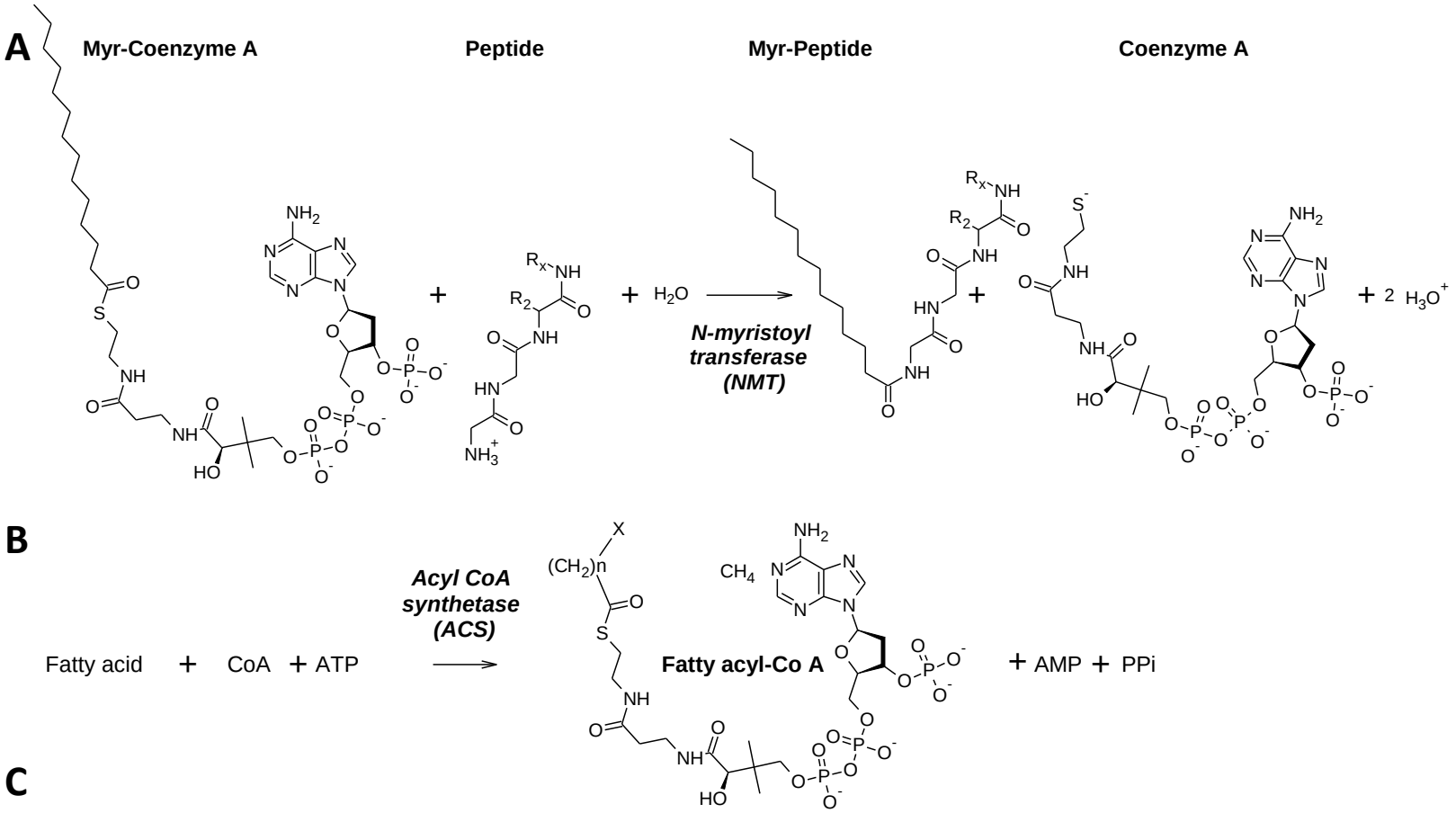
A
Myr-Coenzyme A
Peptide
Myr-Peptide
Coenzyme A
N-myristoyl transferase (NMT)
B
Acyl CoA synthetase (ACS)
Fatty acid + CoA + ATP
Fatty acyl-Co A
+ AMP + PPi
C
Myr-Gly-Peptide
Myr-Gly
Peptide
IpaJ

Fig. 1

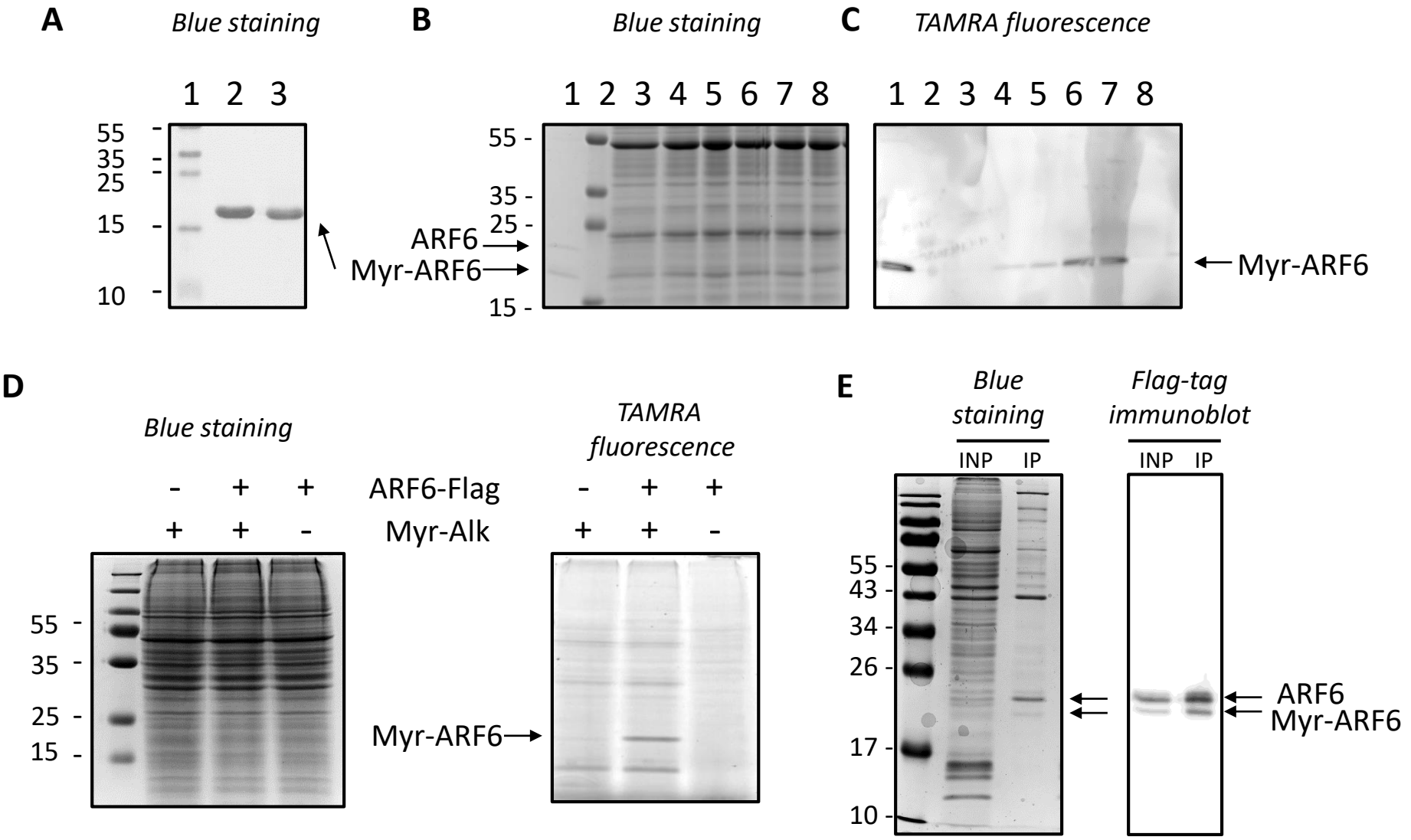
A
Blue staining
1 2 3
55
35
25
15
10
B
Blue staining
1 2 3 4 5 6 7 8
55
35
25
15
ARF6
Myr-ARF6
C
TAMRA fluorescence
1 2 3 4 5 6 7 8
Myr-ARF6
D
Blue staining
TAMRA fluorescence
- + + ARF6-Flag - + +
+ + - Myr-Alk + + -
55
35
25
15
Myr-ARF6
E
Blue staining
Flag-tag immunoblot
INP IP
INP IP
55
43
34
26
17
10
ARF6
Myr-ARF6

Fig. 2

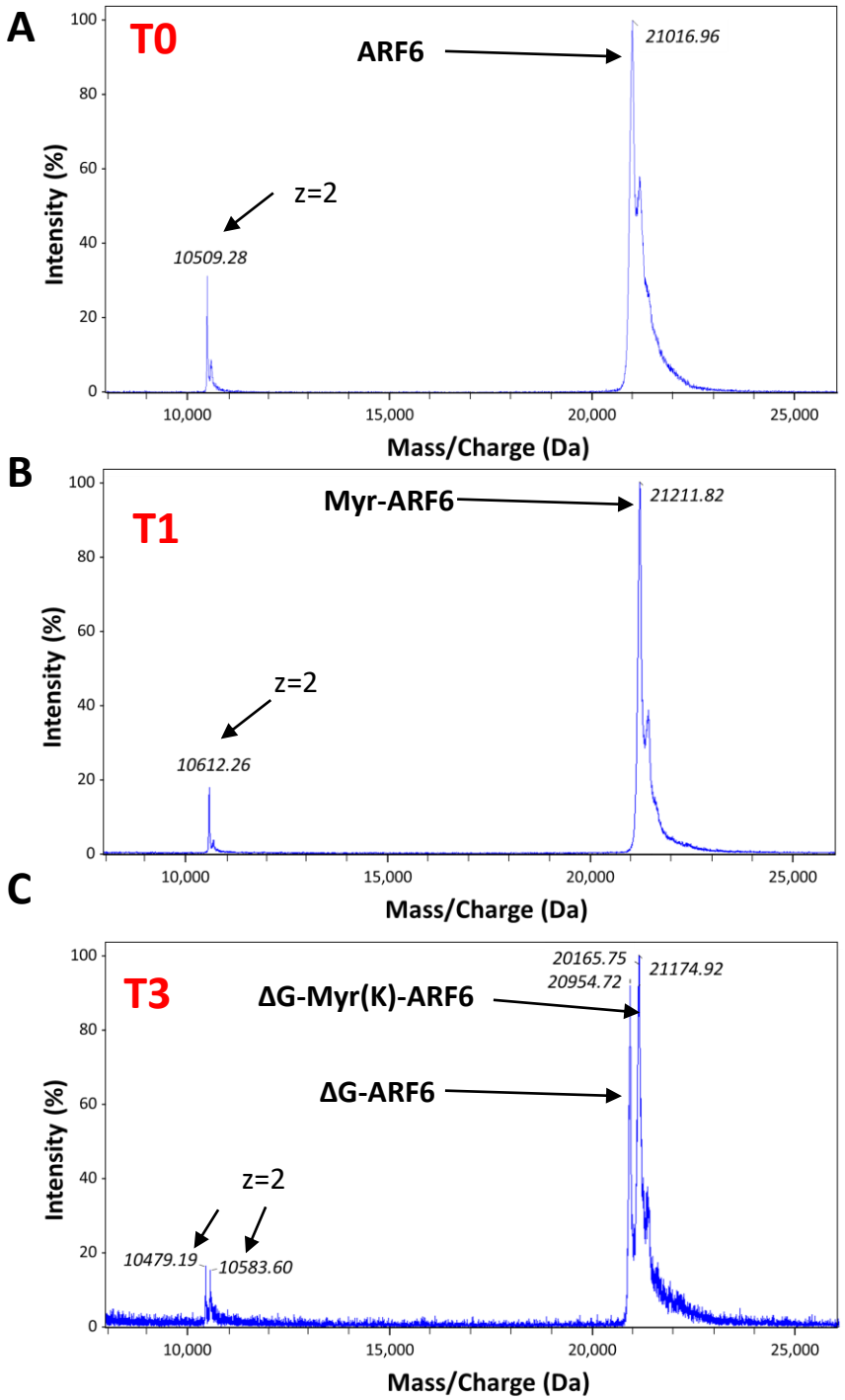

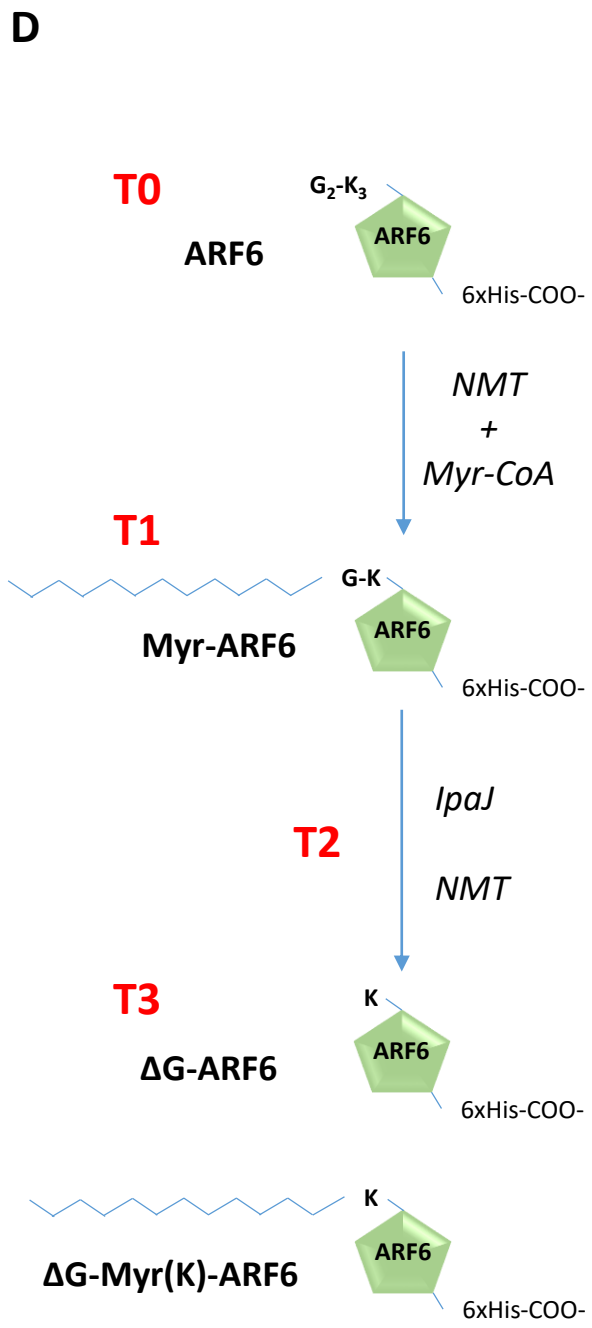

Average masses (Da) ***Mass differences (Da)***

Measured (Me)
Theoretical (Th)

Me: 21,015±3
Th: 21,016

***Me*: 210±5**
***Th*: 210**

Me: 21,225±2
Th: 21,226

***Me*: 266±6**
***Th*: 267**

Me: 20,959±4
Th: 20,959

***Me*: 214±11**
***Th*: 210**

Me: 21,173±7
Th: 21,169

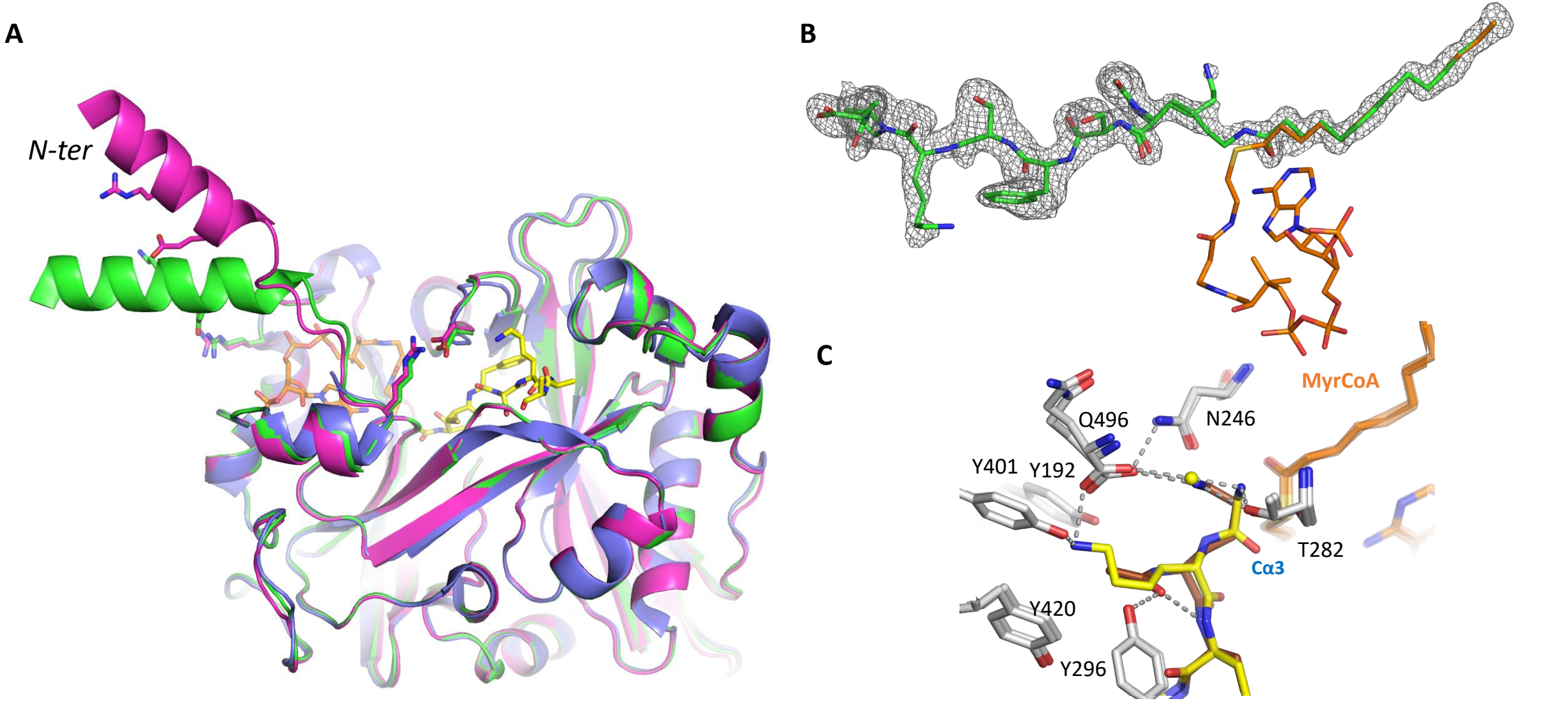

Fig. 4